Imaging δ- and μ-Opioid Receptors by PET in Lung Carcinoma Patients

Igal Madar[1], Badredin Bencherif[1], John Lever[1], Richard F. Heitmiller[2], Stephen C. Yang[2], Malcolm Brock[2], Julie Brahmer[3], Hayden Ravert[1], Robert Dannals[1], and James J. Frost[1]

[1]Department of Radiology, The Johns Hopkins Medical Institutions, Baltimore, Maryland; [2]Department of Surgery, The Johns Hopkins Medical Institutions, Baltimore, Maryland; and [3]Department of Oncology, The Johns Hopkins Medical Institutions, Baltimore, Maryland

In the present study, we measured the kinetics and distribution in vivo of the selective δ-opioid antagonist ^{11}C-methylnaltrindole (^{11}C-MeNTI) and the μ-opioid agonist ^{11}C-carfentanil (^{11}C-CFN) in patients with lung carcinoma using PET. **Methods:** Paired measurements of ^{11}C-MeNTI and ^{11}C-CFN binding were performed in biopsy-proven small-cell ($n = 2$), squamous ($n = 2$), and adenocarcinoma ($n = 3$) lung cancer patients. Dynamic PET scans of increasing duration (0.5–8 min) were acquired over 90 min after an intravenous bolus injection of 370 MBq of tracer. Time–activity curves for tumor and normal lung parenchyma binding were generated using the region-of-interest (ROI) method. The mean activity at equilibrium was measured, and the specific-to-nonspecific binding ratio (tumor − lung)/lung was calculated. Four of 7 patients underwent an additional static ^{18}F-FDG PET scan for clinical indications. Three of 7 patients underwent surgery, and stained sections of tumor were inspected for inflammation, necrosis, and scar tissue. **Results:** Increased binding of ^{11}C-MeNTI and ^{11}C-CFN was detected in all tumor types studied. ^{11}C-MeNTI binding in tumor and healthy lung tissue was significantly more intense than that of ^{11}C-CFN. The average specific-to-nonspecific binding ratio across cell types for ^{11}C-MeNTI (4.32 ± 1.31; mean ± SEM) was greater than that of ^{11}C-CFN (2.42 ± 1.17) but lower than that of ^{18}F-FDG (7.74 ± 0.53). Intravenous naloxone produced 50% and 44% decreases in the specific-to-nonspecific binding ratios of ^{11}C-MeNTI and ^{11}C-CFN, respectively. **Conclusion:** These data provide in vivo evidence for the presence of δ- and μ-opioid receptor types in the 3 major human lung carcinomas and suggest the suitability of ^{11}C-MeNTI and ^{11}C-CFN as investigational probes of lung carcinoma biology.

Key Words: PET; lung carcinoma; opioid receptor

J Nucl Med 2007; 48:207–213

Lung carcinoma continues to be a major health problem of high incidence and high mortality rate, surpassing the mortality of colon, breast, and prostate cancers combined (*1*). Definitive surgery is the most effective treatment for patients with localized, resectable lung tumors. The extent of disease, as determined by tumor staging, is critical in determining patient treatment options and prognosis. Noninvasive imaging has a key role in preoperative evaluation of disease staging. In recent years, major efforts have been made to identify molecular targets in malignant cells and to develop selective probes as diagnostic tools for detection of solid tumors by PET.

In vitro binding assays have shown that small-cell lung carcinoma (SCLC) and non-SCLC cell lines express multiple membrane receptors of μ-, δ-, and κ-types (*2–6*). Investigation of a series of lung cancer cell lines of diverse histologic types suggests that δ-opioid receptors are more abundant than the μ-receptor (*3*). Other studies show a differential distribution of opioid receptor types in lung carcinoma cells. Reverse-transcription polymerase chain reaction of the GLC8 SCLC cell line has found expression of only the δ-opioid receptor (*6*). Reversible binding of the δ-antagonist [^{125}I][H-Tyr(3′-^{125}I)-Tic(ψ)[CH_2NH]Phe-Phe-OH] (ITIPP) was demonstrated in tumor-bearing mice (*7*). Saturable, high-affinity binding sites for μ- and δ-agonists were found in the rat lung parenchyma (*8*). The opioid receptor density in the pulmonary tissue was <10% of that reported for lung carcinoma cell lines.

Over the last 2 decades, our laboratory has developed and characterized several positron-emitting opioid ligands, including the 2 high-affinity PET tracers ^{11}C-carfentanil (^{11}C-CFN), a μ-opioid receptor agonist, and ^{11}C-methylnaltrindole (^{11}C-MeNTI), a δ-opioid receptor antagonist (*9–11*). MeNTI is highly selective for the δ-site (inhibitory concentration = 0.02 nmol/L), it is 700-fold selective for δ- over μ-sites, and it is >3,000-fold selective for δ- over κ-sites (*12*). In mouse brain, ^{11}C-MeNTI binding is inhibited selectively by δ-ligands, but not by μ- or κ-ligands, and the regional distribution correlated well with the established δ-receptor density in vitro (*13*). ^{11}C-MeNTI selectivity for δ-sites was validated in human brain by using quantitative PET (*11*). ^{11}C-CFN is a selective agonist with high affinity for μ-opioid receptors in animal and human brain (*9,10*). ^{11}C-MeNTI and ^{11}C-CFN have been used to localize and quantitate alterations in regional distribution of opioid receptor types associated with various brain disorders (*14–18*).

Received Aug. 22, 2006; revision accepted Oct. 19, 2006.

For correspondence or reprints contact: Igal Madar, PhD, JHOC 4230, 601 N. Caroline St., Baltimore, MD 21287.

E-mail: imadar@jhmi.edu

The objective of the present study was to characterize the biodistribution of ^{11}C-MeNTI and ^{11}C-CFN in the primary tumor and lung tissue in biopsy-proven lung cancer patients with SCLC and non-SCLC of the squamous and adenocarcinoma cell types.

MATERIALS AND METHODS

Patient Characteristics

Seven consecutive newly diagnosed patients (3 male, 4 female; mean age ± SD, 69.1 ± 6.6 y) with biopsy-proven tumor of SCLC or non-SCLC type, tumor size ≥ 2 cm on CT, and no opiate therapy 1 wk or more before the PET studies were entered into the study (Table 1). Informed consent, using guidelines established by the Johns Hopkins University School of Medicine Joint Committee on Clinical Investigation was obtained from each subject before the imaging studies.

Among the 7 patients, there were 2 squamous cancers, 3 adenocarcinomas, and 2 SCLCs (Table 1). Two patients (patients 1 and 7) had a resectable tumor with an extensive chest wall extension. Two patients (patients 2 and 3) had a resectable tumor confined to the lung parenchyma. Two patients (patients 4 and 5) had a nonresectable tumor due to pleural invasion, metastatic disease, and clinical conditions. One patient (patient 6) had a nonresectable SCLC tumor with tumor mass extending from the aortic arch to the main pulmonary artery.

PET Acquisition

Two PET studies were performed on each patient. For 5 subjects, a ^{11}C-MeNTI PET scan, followed by a ^{11}C-CFN PET scan, was acquired. A 1-h rest period between scans was allowed. For 2 subjects, an inhibition study using the opioid antagonist naloxone was performed. The baseline study was followed by the inhibition study with a 1-h rest period between scans. One subject underwent the baseline ^{11}C-MeNTI scan and administration of naloxone (1.0 mg/kg, intravenously) 5 min before commencement of the inhibition scan. The second subject underwent paired ^{11}C-CFN PET scans with administration of 0.16 mg/kg naloxone before commencement of the inhibition scan.

Four of the 7 patients underwent a third PET study of tumor metabolic activity using ^{18}F-FDG. Metabolic imaging was conducted within 3 d before or after opioid receptor studies. There was no treatment during the period between the opioid and metabolic studies. Subjects were positioned in the scanner using the PET laser with the tumor in the center of the scanner field of view (FOV). Positioning of subjects was aided by the anatomic information obtained by the chest CT, by measuring the distance between the sternal notch and the center of the tumor mass.

^{11}C-MeNTI was synthesized via the reaction of ^{11}C-methyliodide with *O*-benzyl-naltrindole (*13*) (injected dose, 640.1 ± 85.1 MBq; specific activity, 83.4 ± 31.4 GBq/μmol). ^{11}C-CFN was synthesized via the reaction of ^{11}C-methyliodide with the normethyl precursor (*19*) (injected dose, 712.6 ± 26.8 MBq; specific activity, 177.7 ± 52.7 GBq/μmol). The mean injected dose of ^{18}F-FDG was 373.1 ± 56.6 MBq.

PET data were acquired on an Advance scanner (GE Healthcare; 35 slices, 4.25-mm thick, 14.4-cm FOV). The patients were placed on the scanner bed, and the PET laser was positioned on the sternal notch; then the bed was moved along the distance measured on the CT scan for centering the tumor in the scanner FOV. A 10-min transmission scan using a ^{68}Ge/^{68}Ga source was performed for subsequent attenuation correction. After intravenous administration of the radiotracer, a series of 25 serial PET images was acquired. The image duration increased progressively from 30 s to 8 min until 90 min after injection. The whole-body ^{18}F-FDG PET scan, commencing 30 min after a bolus injection of the tracer, was performed in 6 bed positions, 8 min per bed position. Subjects were monitored continuously throughout the scanning period for correction of any deviation.

PET Scan Quantification

Scans were corrected for radioactivity decay and for attenuation by using the acquired transmission scan. Reconstruction of images was accomplished by ordered-subset expectation maximization using a 26 × 26 cm FOV, a 256 × 256 pixel matrix (2 × 2 × 4.5 mm voxel size), and a final cubic resolution of 7.8 mm.

Serial images from 0 to 90 min were summed to produce an image for placement of regions of interest (ROIs). The summed images were resampled using linear interpolation to a cubic voxel of 2 mm^3. Images were presented in the coronal plane, and a rectangular ROI (8 × 8 mm) was drawn at the center of the tumor activity profile. The slice representing peak activity in the tumor was selected for further analysis. In some tumors a central area of reduced binding was present. Its diameter was measured on PET from the activity profile across the longitudinal axis as the distance between voxels with value of 50% the difference between tumor maximum activity and mean activity of the surrounding tissue. In 1 subject (patient 6), having a large tumor (6 × 8 × 4 cm), the area of increased receptor binding was interrupted, and tracer tumor uptake was sampled by 3 ROIs. In the remaining subjects, a continuous distribution of radioligands throughout the tumor area was observed, and tumor tracer uptake was sampled by a single ROI. Nontumor radioactivity was quantified by placing a rectangular ROI on the healthy lung parenchyma above and below the tumor mass and on the contralateral lung in a position

TABLE 1
Patient Characteristics

Patient no.	Age (y)	Sex	Clinical stage	Surgical resection	Cell type	Tumor size (cm)	Tumor localization
1	66	M	IIb	Yes	Squamous	8 × 3 × 3	L upper lobe
2	72	M	IIb	Yes	Squamous	4 × 5 × 2	L upper lobe
3	72	F	I	Yes	Adenocarcinoma	3 × 2 × 2	L upper lobe
4	66	F	IIb	No	Adenocarcinoma	4 × 3 × 4	R upper lobe
5	75	F	IIb	No	Adenocarcinoma	2 × 4 × 2	R middle lobe
6	57	F	IIIa	No	SCLC	6 × 8 × 4	L middle lobe
7	76	M	IIb	Yes	SCLC	3 × 2 × 3	L upper lobe

corresponding to the ROIs ipsilateral to the malignant lesion (total number of ROIs = 6). The ROI template was transferred to the serial images of the corresponding PET section, and time–activity curves of tracer in tumor and healthy lung tissue were plotted. Image-processing procedures were performed using Analyze software (Mayo Clinic, Rochester, MN).

The time–activity curves were used to determine time-to-plateau activity. In all subjects, ^{11}C-MeNTI and ^{11}C-CFN activity in tumor plateaued over the 50- to 90-min postinjection time interval (Fig. 1). For each ROI, the mean radioactivity over the 50- to 90-min time interval was calculated from the corresponding time−radioactivity curves. The ROIs' counts/cm^3/min were normalized to the injected dose (Bq/cm^3/MBq injected). In addition, counts were translated to standardized uptake value (SUV) per body weight ([kBq/cm^3/MBq] × kg).

In some tumors, a necrotic core was present. An assessment of the core diameter was obtained by generating the activity profile across the tumor long axis and surrounding healthy tissue. The core boundaries were determined as 50% of the difference between the minimum activity in the tumor area and the mean activity in the normal surrounding tissue. The Student t test was used to test the hypothesis of significant differences between ^{11}C-MeNTI and ^{11}C-CFN binding and between tumor and nontumor structures. Differences with $P < 0.05$ were judged as significant.

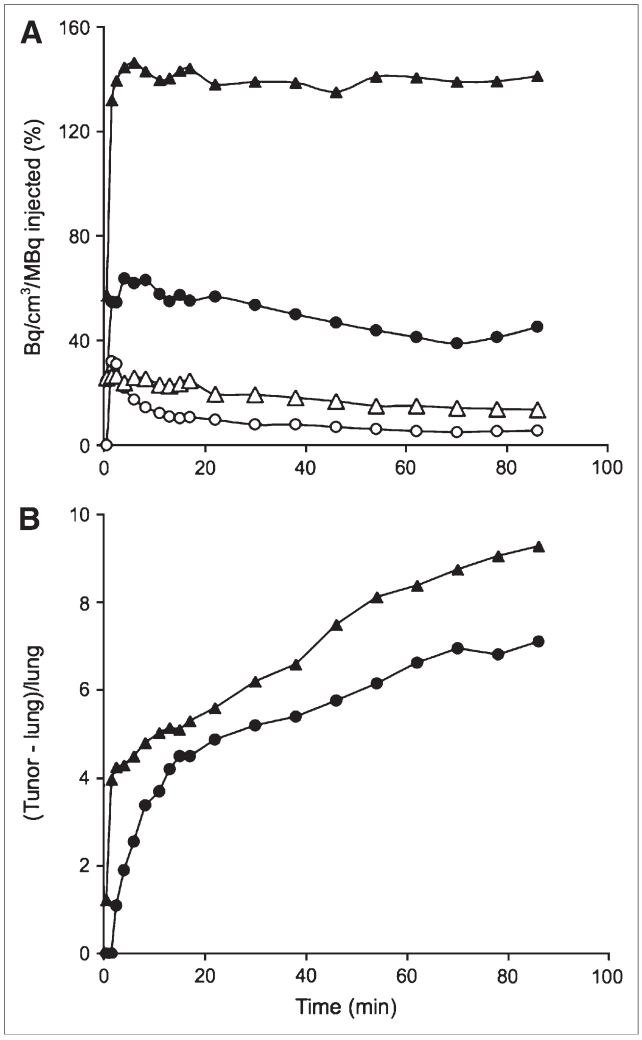

FIGURE 1. Kinetics of ^{11}C-MeNTI and ^{11}C-CFN tumor binding in non-SCLC patient. (A) Radioligand activity in tumor (MeNTI, ▲; CFN, ●) and host lung tissue (MeNTI, △; CFN, ○). Activity in healthy lung represents mean of 5 ROIs. (B) Specific-to-nonspecific binding ratio. ^{11}C-MeNTI activity (▲) in tumor is significantly greater than that in ^{11}C-CFN (●). ^{11}C-MeNTI and ^{11}C-CFN binding reaches plateau in tumor but decreases gradually in nonmalignant lung tissue; consequently, specific-to-nonspecific binding ratios for both radioligands increase continuously.

RESULTS

Tumor Characteristics

The extent of inflammation, necrosis, and scarring in the tumor area was evaluated on 7-μm hematoxylin- and eosin-stained histologic sections of surgical specimens of 3 patients, as summarized in Table 2. One patient (patient 3) demonstrated a focal central scar (0.5 cm) and desmoplasia with cystic changes accompanied with arterial occlusion by tumor thrombosis. One patient (patient 1) demonstrated intermediate chronic as well as intense acute inflammation in some regions with a focal abscess formation; a 2-cm scar in lung parenchyma surrounded by viable tumor cells and obliteration of large-caliber lobar arteries were observed in the scar region. One patient (patient 7) demonstrated extensive necrosis with zones of viable cells measuring up to 0.5 cm at the tumor margin.

^{11}C-MeNTI and ^{11}C-CFN Binding Kinetics

An example of a time–activity profile for ^{11}C-MeNTI and ^{11}C-CFN binding in tumor and healthy lung parenchyma obtained in SCLC tumor (patient 6) is shown in Figure 1A. In tumor, ^{11}C-MeNTI and ^{11}C-CFN binding reach a plateau within a few minutes, which is maintained throughout most of the scanning period (90 min). ^{11}C-MeNTI plateaus at significantly greater values than does ^{11}C-CFN. In some tumors, binding kinetics were slower than those observed in Figure 1 but, in all subjects, plateau activity was obtained during the 50- to 90-min period. In contrast, ^{11}C-MeNTI and ^{11}C-CFN activity in healthy lung parenchyma, after an early peak, gradually washed out throughout the scanning time (Fig. 1A). A washout of activity from the healthy pulmonary tissue was observed in

TABLE 2
Histopathology of Lung Carcinoma

Patient no.	Inflammation	Scarring	Necrosis
3	0/3	1/3 (0.5 cm)	0/3
7	0/3	0/3	3/3
1	Chronic, 1–2/3; acute, 2/3	1–2/3, desmoplesia; 2-cm scar	0/3

Histopatholgies are graded 0–3: 0 = no pathology and 3 = severe pathology.

all subjects for both ^{11}C-MeNTI and ^{11}C-CFN. Figure 1B depicts the specific-to-nonspecific activity ratio, calculated as (tumor − lung)/lung, which increased linearly with time for both ^{11}C-MeNTI and ^{11}C-CFN.

Inhibition Study

The opioid antagonist naloxone produced a significant decrease of ^{11}C-MeNTI and ^{11}C-CFN tumor binding. Figure 2 demonstrates the effect of intravenous administration of naloxone on the time–activity profiles of ^{11}C-MeNTI in adenocarcinoma primary tumor and healthy pulmonary tissue (patient 4). In the absence of naloxone (Fig. 2A), ^{11}C-MeNTI binding in tumor rapidly plateaued, whereas binding in healthy lung parenchyma gradually declined. In contrast, intravenous administration of naloxone produced a significant washout of radioligand from tumor at a rate similar to that observed in the healthy lung parenchyma. Naloxone did not affect ^{11}C-MeNTI binding kinetics in the healthy lung tissue (Fig. 2B). A similar effect of naloxone on binding kinetics of ^{11}C-CFN in tumor and healthy lung parenchyma was observed. Administration of naloxone at a dose of 1.0 mg/kg resulted in a 50% decrease of the specific-to-nonspecific binding ratio for ^{11}C-MeNTI, whereas a lesser dose (0.16 mg/kg) was required to exert a comparable inhibition (44%) of ^{11}C-CFN binding ratio.

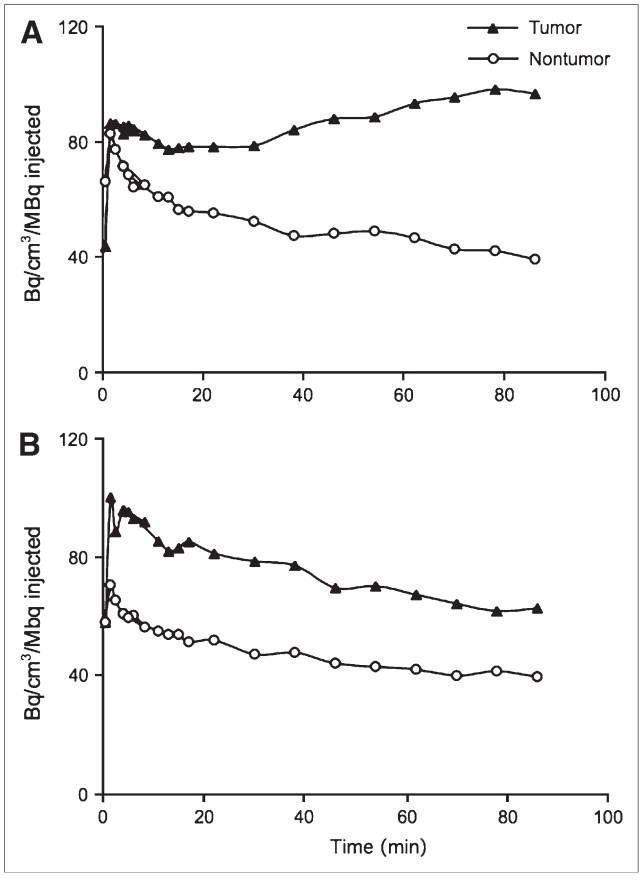

FIGURE 2. Effect of intravenous naloxone on ^{11}C-MeNTI kinetics in lung adenocarcinoma (patient 4). Traces represent activity profile of ^{11}C-MeNTI in tumor (▲) and healthy lung tissue (○) in absence (A) and presence (B) of naloxone. Nontumor represents mean of 5 samplings, using rectangular (8 × 8 mm) ROI, of activity in healthy lung parenchyma. Naloxone produces washout of binding in tumor but does not affect pharmacokinetics in normal lung.

Tumor Uptake

Elevated tumor binding of ^{11}C-MeNTI and ^{11}C-CFN was detected in all but 1 subject (patient 7) with a large necrotic core in tumor (Table 3). The mean ^{11}C-MeNTI tumor's SUV, across subjects, was 7.4 ± 0.85 (mean ± SEM) compared with 1.8 ± 0.44 in the healthy lung tissue. ^{11}C-CFN binding in tumor was significantly ($P = 0.003$) lower than that of ^{11}C-MeNTI. The average ^{11}C-CFN SUVs in tumor and host lung were 2.7 ± 0.72 and 0.91 ± 0.25, respectively. Consequently, the mean specific-to-nonspecific binding ratio, was greater for ^{11}C-MeNTI (4.32 ± 1.30) than that for ^{11}C-CFN (2.42 ± 1.17). The mean ^{18}F-FDG SUVs in tumor and host lung were 5.7 ± 1.29 and 0.66 ± 0.14, respectively (Table 3).

The distribution of receptor binding across the tumor area was not uniform. In 3 patients (patients 1–3), intense opioid receptor binding was confined to the margin of the tumor, composing a ring of increased binding surrounding a central cold area. In 2 other patients (patients 4 and 6), regions of increased receptor binding were distributed in discrete patches throughout the tumor mass. Figure 3 demonstrates a coronal view of PET images acquired from a patient with a squamous lung carcinoma tumor (patient 1). The tumor mass was localized in the lateral upper left lobe invading the chest wall. ^{11}C-MeNTI and ^{11}C-CFN binding comprises a rim of increased activity in the medial aspect of the tumor with no binding in the tumor core or in the tumor lateral aspect of the tumor bordering the chest wall.

In 4 patients, the distribution of the opioid receptor binding was compared with the tumor ^{18}F-FDG uptake. In 2 of 4 patients (patients 1 and 2), increased uptake of ^{18}F-FDG was confined to the tumor margin, similar to the distribution pattern observed by opioid receptor studies (Fig. 3). However, the central core of decreased receptor binding was larger than the metabolic cold center. In the example shown in Figure 3, the cold center diameter in the long axis is 38 and 13 mm for ^{11}C-MeNTI and ^{18}F-FDG studies, respectively. The opioid receptor cold spot was also larger than the necrotic core, as measured on histologic sections and the cavity observed on the CT scans. In 2 patients, a necrotic core of 20 and 5 mm was measured on CT, whereas the opioid receptor cold spot was 38 and 10 mm in diameter. ^{11}C-MeNTI and ^{11}C-CFN binding sites demonstrated similar distribution across the malignant tissue, and the region of reduced binding was of a similar diameter.

In 3 patients, tumor histologic sections were inspected for the presence of tumor infiltrating macrophages and lymphocytes and visually compared with the distribution of ^{11}C-MeNTI and ^{11}C-CFN. Immune cells were detected in

TABLE 3
Tumor and Lung Binding of ^{11}C-MeNTI, ^{11}C-CFN, and ^{18}F-FDG

Patient no.	Cell type	Bq/cm^3/MBq		SUV		Ratio	
		Tumor	Nontumor	Tumor	Nontumor	T/NT	SP/NSP
			^{11}C-MeNTI				
1	Squamous	82.7*	22.70	9.55	2.62	3.65	2.64
2	Squamous	98.3	29.35	8.85	2.64	3.35	2.35
3	Adenocarcinoma	70.6	10.55	4.65	0.70	6.69	5.69
4	Adenocarcinoma	99.4	32.25	6.78	2.20	3.08	2.08
6	SCLC	140.2	14.25	7.26	0.74	9.84	8.84
7	SCLC	No uptake due to extensive necrosis					
			^{11}C-CFN				
1	Squamous	40.4	13.54	4.66	1.56	2.99	1.98
2	Squamous	39.2	15.50	3.53	1.40	2.53	1.53
3	Adenocarcinoma	4.8	5.66	0.32	0.37	0.85	−0.15
5	Adenocarcinoma	35.1	12.10	2.79	0.96	2.91	1.90
6	SCLC	42	5.35	2.18	0.28	7.85	6.85
7	SCLC	No uptake due to extensive necrosis					
			^{18}F-FDG				
1	Squamous	41.93	4.13	4.84	0.48	10.15	9.15
2	Squamous	52.33	6.17	4.71	0.56	8.49	7.49
4	Adenocarcinoma	57.60	7.67	3.80	0.51	7.51	6.51
5	Adenocarcinoma	120.08	13.65	9.55	1.09	8.80	7.80

*Mean activity over 60–90 min.
T/NT = tumor/nontumor ratio; SP = specific activity (tumor − nontumor); NSP = nonspecific activity (mean of 5 ROIs, 2 ipsilateral and 3 contralateral to tumor).

only 1 patient. Their distribution did not correspond with the distribution of ^{11}C-MeNTI or ^{11}C-CFN binding.

DISCUSSION

This study provides in vivo evidence for the presence of μ- and δ-opioid receptors in human lung carcinoma, using the receptor type–selective tracers ^{11}C-MeNTI and ^{11}C-CFN and PET. The results of this study suggest that opioid receptors are significantly more abundant in lung carcinoma than in the normal host tissue and that the relative increase in δ-opioid binding sites in malignant lesions is greater than that of the μ-opioid subtype.

Expression of Opioid Binding Sites in Lung Carcinoma

Several lines of evidence indicate the selectivity of ^{11}C-MeNTI and ^{11}C-CFN for their related δ- and μ-opioid receptor types in lung carcinomas tumor. First, the linear increase in the specific component of tracer binding in tumor, as well as the washout of activity from the normal lung parenchyma, is typical of kinetics observed for ^{11}C-MeNTI and ^{11}C-CFN in opioid receptor-rich and -poor regions in the human brain, respectively, (*10,11,20*). This finding is in line with the abundance of δ-opioid (800 fmol/mg protein) and μ-opioid (1,700 fmol/mg) receptors in lung carcinoma cell lines (*3*), compared with the paucity of the opioid receptor density in lung parenchyma cells, measured in rats (3 and 150 fmol/mg protein, respectively) (*8*).

Second, the mean tumor-to-nontumor uptake ratio was significantly greater for ^{11}C-MeNTI than that for ^{11}C-CFN. This finding confirms in vitro reports, suggesting that receptor binding in lung carcinoma cells, normalized to healthy parenchymal cells, is much greater for δ- than for μ-opioid–selective radioligands (*3,8*).

Third, administration of the opioid antagonist naloxone reduced the binding in tumor but did not affect the activity in the healthy lung tissue. This finding suggests that activity in healthy lung is primarily nonspecific. In addition, naloxone produced comparable inhibition of ^{11}C-MeNTI and ^{11}C-CFN binding. However, the naloxone dose required to exert comparable inhibition was 5 times greater for ^{11}C-MeNTI than that for ^{11}C-CFN. This finding suggests a relatively greater density of δ-opioid receptors. In the human brain, the inhibitory potency of the opioid antagonist naltrexone was directly correlated ($R^2 = 0.88$) with the regional density of δ-sites (*11*).

Comparison of Expression of Opioid Binding Sites in Lung Tumor and Brain

Previously, ^{11}C-MeNTI and ^{11}C-CFN were used for the quantification of opioid binding sites in the human brain by PET (*9–11,20,21*). Comparison between these studies and the present work reveals interesting differences in the distribution of opioid binding sites. In the human brain, μ-opioid receptors are predominant compared with δ-receptors, whereas in lung carcinoma a reversed relationship was found.

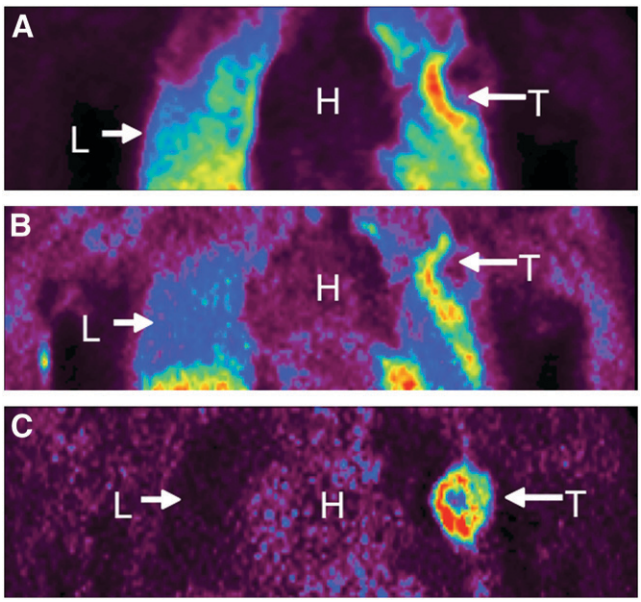

FIGURE 3. Coplanar coronal sections of ^{11}C-MeNTI (A), ^{11}C-CFN (B), and ^{18}F-FDG (C) PET images acquired in a patient with squamous lung carcinoma (patient 1): an 8 × 3 × 3 cm tumor, localized in lateral aspect of upper left lobe, extending to chest wall. Increased ^{11}C-MeNTI and ^{11}C-CFN binding forms an arch surrounding a cold center. Quantitative values obtained at the peak activity profile of the tumors are presented in Table 3. All 3 tracers demonstrate reduced binding in lateral aspect of the tumor bordering the chest wall, but this decrease is more pronounced for the δ-opioid receptors. Likewise, all 3 tracers demonstrate reduced activity at the tumor center, but this area is larger for the opioid agents. ^{11}C-MeNTI binding in tumor and healthy lung is more intense than that of ^{11}C-CFN. L = lung; H = heart; T = tumor.

The absolute amount of ^{11}C-MeNTI binding to δ-opioid receptors in lung carcinoma (98.2 Bq/cm^3/MBq) was 3 times greater than that measured in brain regions known to contain high δ-receptor density (30 Bq/cm^3/MBq) (*11*). In contrast, ^{11}C-CFN binding in lung carcinoma tumor was significantly less than that in the human brain (27.5 Bq/cm^3/MBq in tumor vs. 50 Bq/cm^3/MBq in thalamus). Moreover, this difference is even more accentuated when the tracer's binding is expressed as the specific-to-nonspecific activity ratio, a measure of opioid receptors' binding potential (dissociation constant/maximum number of binding sites) (*21*). In lung carcinoma tumor, the δ-receptor binding potential is 6 times greater than that in receptor-rich brain regions (4.3 vs. 0.73), whereas this ratio for ^{11}C-CFN is about half that in the brain (2.4 vs. 5.1) (*11*). This finding is in line with in vitro reports. δ-Receptor concentration in human brain, as determined by quantitative autoradiography, is in the range of a few picomoles per gram of protein (*22*), whereas receptor density in lung carcinoma cell lines is in the range of a several hundreds of picomoles per gram (*3*).

Potential Clinical Implications

In addition to their analgesic effect, opioids appear to be important in the growth regulation of normal and neoplastic tissue (*23*). Opioid alkaloids, endogenous opioid analogs, and food-derived opioid peptides inhibit in a dose-dependent manner the proliferation of a wide diversity of human tumors (*24*), including lung carcinoma cells (*3,25–27*). Expression of opioid binding sites correlated inversely with tumor growth in vivo, and administration of opioid agonists resulted in increased survival rates of tumor-bearing mice (*28*). In lung, colon, and breast carcinoma cells, opioid-induced growth suppression was associated with elevated expression of apoptosis markers (*29*). Opioid agonists potentiated the antitumor activity of paclitaxel (*30*). The well-documented negative growth effect suggests that ^{11}C-MeNTI and ^{11}C-CFN PET may afford an effective diagnostic tool of important prognostic value. Currently, opioid-based anticancer drugs are in early clinical trials (*31*). Opioid receptor imaging using PET may facilitate the development of future anticancer drugs and assist in selecting proper candidates for treatment using opioid peptides.

Animal studies have shown that opioids may not only suppress proliferation but also affect migration and invasive activity of neoplastic cells (*32*). Migration of immune and neoplastic cells are modulated by μ- and δ-opioid peptides acting as chemoattractants (*33*). Moreover, opioid peptides were implicated in the invasive activity of neoplastic cells either by remodeling actin cytoskeleton associated with phosphorylation of δ-opioid receptors or by enzymatic degradation of the extracellular matrix (*34,35*). These data may attribute functional significance to the localization of opioid binding sites to the tumor margin as observed in most patients in the present study. The finding that the region of reduced receptor binding was much larger than the histopathologic or radiographic core or the hypometabolic region suggests that the unique distribution of opioid receptors in lung tumors is not dictated solely by viability factors. Neoplastic cells involved in metastatic spreading or attraction of immune cells will most likely be localized in the tumor margin. However, further PET studies in a larger group of patients are needed to explore the relationship between opioid receptors and tumor proliferation and metastatic activity. Elucidation of the role of opioids in paracrine interactions between tumor cells and the surrounding tissue may propose a new noninvasive diagnostic tool of important prognostic significance in lung cancer and other types of solid tumors.

CONCLUSION

PET of specific opioid receptor-type probes provides evidence that SCLC and non-SCLC in humans express high levels of both δ- and μ-opioid types. δ-Receptors are more abundant than the μ-type across the 3 major lung carcinoma types. Both receptor types appear mainly in the tumor margin, suggesting a functional role of the nonbrain opioid system. Quantitative imaging of opioid receptor subtypes in patients may further the understanding of lung cancer biology and extend the biochemical characterization of

individual tumors—thereby, improving prognosis and treatment of solid carcinomas.

ACKNOWLEDGMENTS

The authors thank Drs. William Mathews and John Musachio for assisting in the radiosyntheses, David Clough and Karen Edmonds for their assistance in the PET imaging procedures, and Martin Stumpf for managing the data systems. This research was supported, in part, by National Cancer Institute grant CA 32845.

REFERENCES

1. Parkin DM, Bray FI, Devesa SS. Cancer burden in the year 2000: the global picture. *Eur J Cancer.* 2001;37(suppl 8):4–66.
2. Campa MJ, Schreiber G, Bepler G, et al. Characterization of delta opioid receptors in lung cancer using a novel nonpeptidic ligand. *Cancer Res.* 1996;56:1695–1701.
3. Maneckjee R, Minna JD. Opioid and nicotine receptors affect growth regulation of human lung cancer cell lines. *Proc Natl Acad Sci U S A.* 1990;87:3294–3298.
4. Roth KA, Barchas JD. Small cell carcinoma cell lines contain opioid peptides and receptors. *Cancer.* 1986;57:769–773.
5. Schreiber G, Campa MJ, Prabhakar S, et al. Molecular characterization of the human delta opioid receptor in lung cancer. *Anticancer Res.* 1998;18:1787–1792.
6. Sher E, Codignola A, Passafaro M, et al. Nicotinic receptors and calcium channels in small cell lung carcinoma: functional role, modulation, and autoimmunity. *Ann N Y Acad Sci.* 1998;841:606–624.
7. Collier TL, Schiller PW, Waterhouse RN. Radiosynthesis and in vivo evaluation of the pseudopeptide delta-opioid antagonist [^{125}I]ITIPP(psi). *Nucl Med Biol.* 2001;28:375–381.
8. Bhargava HN, Villar VM, Cortijo J, Morcillo EJ. Binding of [^{3}H][D-Ala^{2},MePhe^{4},Gly-ol^{5}]enkephalin, [^{3}H][D-Pen^{2} D-Pen^{5}]enkephalin, and [^{3}H]U-69,593 to airway and pulmonary tissues of normal and sensitized rats. *Peptides.* 1997;18:1603–1608.
9. Frost JJ, Dannals RF, Duelfer T, et al. In vivo studies of opiate receptors. *Ann Neurol.* 1984;15(suppl):S85–S92.
10. Frost JJ, Douglass KH, Mayberg HS, et al. Multicompartmental analysis of ^{11}C-carfentanil binding to opiate receptors in humans measured by positron emission tomography. *J Cereb Blood Flow Metab.* 1989;9:398–409.
11. Madar I, Lever JR, Kinter CM, et al. Imaging of delta opioid receptors in human brain by N1′-(^{11}C-methyl)naltrindole and PET. *Synapse.* 1996;24:19–28.
12. Portoghese PS, Sultana M, Takemori AE. Design of peptidomimetic delta opioid receptor antagonists using the message-address concept. *J Med Chem.* 1990;33:1714–1720.
13. Lever JR, Kinter CM, Ravert HT, Musachio JL, Mathews WB, Dannals RF. Synthesis of N1′-(^{11}C-methyl)naltrindole (^{11}C-MeNTI): a radioligand for positron emission tomographic studies of delta opioid receptors. *J Labelled Compds Radiopharm.* 1995;36:137–145.
14. Bencherif B, Stumpf M, Wang G, McCaul M, Madar I, Frost J. Brain mu opioid receptor binding changes in chronic alcoholics before and after partial volume correction (PVC) [abstract]. *J Nucl Med.* 2001;42(suppl):107P.
15. Madar I, Bencherif B, Brandt J, Rabins PV, Zubeita JK, Frost JJ. Mu opioid receptors in Alzheimer's disease: statistical parametric mapping analysis [abstract]. *J Nucl Med.* 2001;42(suppl):12P.
16. Madar I, Lesser RP, Krauss G, et al. Imaging of delta- and mu-opioid receptors in temporal lobe epilepsy by positron emission tomography. *Ann Neurol.* 1997;41:358–367.
17. Frost JJ, Mayberg HS, Fisher RS, et al. Mu-opiate receptors measured by positron emission tomography are increased in temporal lobe epilepsy. *Ann Neurol.* 1988;23:231–237.
18. Zubieta JK, Gorelick DA, Stauffer R, Ravert HT, Dannals RF, Frost JJ. Increased mu opioid receptor binding detected by PET in cocaine-dependent men is associated with cocaine craving. *Nat Med.* 1996;2:1225–1229.
19. Dannals RF, Ravert HT, Frost JJ, Wilson AA, Burns HD, Wagner HN Jr. Radiosynthesis of an opiate receptor binding radiotracer: ^{11}C-carfentanil. *Int J Appl Radiat Isot.* 1985;36:303–306.
20. Smith JS, Zubieta JK, Price JC, et al. Quantification of delta-opioid receptors in human brain with N1′-(^{11}C-methyl)naltrindole and positron emission tomography. *J Cereb Blood Flow Metab.* 1999;19:956–966.
21. Endres CJ, Bencherif B, Hilton J, Madar I, Frost JJ. Quantification of brain mu-opioid receptors with [^{11}C]carfentanil: reference-tissue methods. *Nucl Med Biol.* 2003;30:177–186.
22. Pfeiffer A, Pasi A, Mehraein P, Herz A. Opiate receptor binding sites in human brain. *Brain Res.* 1982;248:87–96.
23. Zagon IS, McLaughlin PJ. Opioids and differentiation in human cancer cells. *Neuropeptides.* 2005;39:495–505.
24. Hatzoglou A, Kampa M, Castanas E. Opioid-somatostatin interactions in regulating cancer cell growth. *Front Biosci.* 2005;10:244–256.
25. Munjal I, Minna J, Maneckjee R, Bieck P, Spector S. Possible role of endogenous morphine and codeine on growth regulation of lung tissue. *Life Sci.* 1995;57:517–521.
26. Heusch WL, Maneckjee R. Signalling pathways involved in nicotine regulation of apoptosis of human lung cancer cells. *Carcinogenesis.* 1998;19:551–556.
27. Maneckjee R, Minna JD. Opioids induce while nicotine suppresses apoptosis in human lung cancer cells. *Cell Growth Differ.* 1994;5:1033–1040.
28. Gomez-Flores R, Caballero-Hernandez D, Tamez-Guerra R, et al. Increased survival of tumor-bearing mice by the delta opioid SNC 80. *Anticancer Res.* 2005;25:4563–4567.
29. Hatsukari I, Hitosugi N, Matsumoto I, Nagasaka H, Sakagami H. Induction of early apoptosis marker by morphine in human lung and breast carcinoma cell lines. *Anticancer Res.* 2003;23:2413–2417.
30. Jaglowski JR, Zagon IS, Stack BC Jr. Opioid growth factor enhances tumor growth inhibition and increases the survival of paclitaxel-treated mice with squamous cell carcinoma of the head and neck. *Cancer Chemother Pharmacol.* 2005;56:97–104.
31. Smith JP, Conter RL, Bingaman SI. Treatment of advanced pancreatic cancer with opioid growth factor: phase I. *Anticancer Drugs.* 2004;15:203–209.
32. McLaughlin PJ, Zagon IS. Progression of squamous cell carcinoma of the head and neck is associated with down-regulation of the opioid growth factor receptor. *Int J Oncol.* 2006;28:1577–1583.
33. Fichna J, Janecka A. Opioid peptides in cancer. *Cancer Metastasis Rev.* 2004;23:351–366.
34. Entschladen F, Bastian P, Niggemann B, Zaenker KS, Lang K. Inhibition of cell migration via G protein-coupled receptors to opioid peptides and angiotensin. *Ann N Y Acad Sci.* 2004;1028:320–328.
35. Harimaya Y, Koizumi K, Andoh T, Nojima H, Kuraishi Y, Saiki I. Potential ability of morphine to inhibit the adhesion, invasion and metastasis of metastatic colon 26-L5 carcinoma cells. *Cancer Lett.* 2002;187:121–127.